



Chalcophile element fertility and the formation of porphyry Cu ± Au deposits

Jung-Woo Park^{1,2} · Ian H. Campbell² · Sanjeeva P. K. Malaviarachchi³ · Helen Cocker² · Hongda Hao² · Suzanne M. Kay⁴

Received: 21 February 2018 / Accepted: 5 August 2018 / Published online: 8 September 2018
© The Author(s) 2018

Abstract

Chalcophile element fertility, the chalcophile metal abundance in the source magma, is likely to be a critical factor for the formation of porphyry Cu ± Au deposits. In this study, we provide evidence to support this hypothesis by comparing the platinum group element (PGE) geochemistry of barren and ore-bearing Cu ± Au granitic suites. We report the PGE contents of three barren volcanic and subvolcanic suites from Argentina and Japan and two Cu ± Au bearing suites from Indonesia and Chile. These results are compared with those from previous studies of a porphyry Cu-only subvolcanic suite from Chile and three porphyry Cu-Au-bearing suites from Australia and the USA. The barren suites are depleted in PGE abundances by the time of fluid exsolution (< 0.1 ppb Pd and Pd/Pt < ~ 3), which is attributed to early sulfide saturation in a mid to lower crustal magma chamber. In contrast, the Cu ± Au ore-bearing suites contain at least an order of magnitude higher PGE contents than the barren ones at fluid saturation (up to ~ 10 ppb Pd and Pd/Pt of 0.1–40). They are characterized by late sulfide saturation, which allows both chalcophile elements and sulfur to concentrate by fractional crystallization before volatile saturation. We suggest that plots of Pd/MgO against Pd/Pt for igneous suites can be used to estimate chalcophile element fertility and distinguish between barren, porphyry Cu, and porphyry Cu-Au granitoid systems. The positive correlation of these chalcophile element fertility indicators and ore grades suggests that metal contents in magmas play an important role in controlling ore grade, particularly Au, in porphyry Cu ± Au deposits.

Keywords Platinum group element · Porphyry deposit · Chalcophile element fertility · Sulfide saturation

Editorial handling: W. D. Maier

Electronic supplementary material The online version of this article (<https://doi.org/10.1007/s00126-018-0834-0>) contains supplementary material, which is available to authorized users.

✉ Jung-Woo Park
jung-woo.park@snu.ac.kr

- ¹ School of Earth and Environmental Sciences, Seoul National University, Seoul 08826, South Korea
- ² Research School of Earth Sciences, Australian National University, Canberra, ACT 2601, Australia
- ³ Department of Geology, Faculty of Science, University of Peradeniya, Peradeniya, Peradeniya 20400, Sri Lanka
- ⁴ Earth and Atmospheric Sciences, Cornell University, Ithaca, NY 14853, USA

Introduction

Porphyry deposits are the primary source of the world's Cu and Au. The metals are interpreted to have been deposited from magmatic fluids exsolved from the ore-associated porphyries (Burnham 1967). They predominantly occur above subduction zones, which has led to the suggestion that oxidized, water-rich subduction zone magmas may play an essential role in ore formation. However, only a limited number of porphyry suites host economic deposits. Most are barren. There are several critical factors required to form a large porphyry deposit: the metal endowment of the primary magma (McInnes et al. 1999; Mungall 2002), the metal content of the evolved magma at the time of volatile exsolution (Jenner et al. 2010; Wilkinson 2013; Park et al. 2015), the efficient transfer and precipitation of the ore metals by the magmatic fluid (Richards 2003;

Audétat and Simon 2012; Wilkinson 2013), and the volume of magma and the duration of magmatic activity (Chelle-Michou et al. 2017; Chiaradia and Caricchi 2017). Metal transfer by degassing from a deep to shallow magma chamber (Halter et al. 2005; Chiaradia et al. 2012) and destabilization of magmatic sulfide (Nadeau et al. 2010; Mungall et al. 2015) have also been suggested as contributing factors in ore formation.

The chalcophile metal contents in a magma, the chalcophile element fertility, at the point of fluid exsolution have been considered to be one of the key factors in the formation of porphyry Cu \pm Au deposits (e.g., Wilkinson 2013), but there is no empirical evidence supporting this hypothesis. This is mainly due to the difficulties in measuring the metal contents of the magma from which the ore-forming fluid exsolved. The Cu and Au contents of igneous rocks, particularly those associated with porphyry Cu \pm Au deposits, are often remobilized by hydrothermal alteration and do not reflect magmatic composition.

Recent studies on platinum group element (PGE) geochemistry of subvolcanic rocks associated with porphyry Cu \pm Au deposits (Cocker et al. 2015; Hao et al. 2017; Lowczak et al. 2018) have suggested that the relative timing of fluid and sulfide saturation plays an important role in the formation of porphyry Cu \pm Au deposits. These studies used PGEs to indicate chalcophile element fertility at fluid saturation. The PGEs are used in preference to Cu and Au for two reasons. First, their partition coefficients in immiscible sulfide melts are one to two orders of magnitude higher than those of Cu and Au respectively (Mungall and Brennan 2014). Second, because they are appreciably less affected by alteration than Cu and Au, they are more likely to preserve original igneous geochemistry (e.g., Crocket 2000; Park et al. 2016).

In this paper, we evaluate the role of chalcophile element fertility in determining the ore-forming potential of porphyry systems by comparing the PGE geochemistry of barren suites with that of economic Cu and Cu-Au suites. We measured PGE contents of three barren volcanic and intrusive suites, the Rachaite suite from Argentina, and the Ryoke and Sanyo ilmenite-series and Sanin magnetite-series granitoids from Japan (Fig. 1). We also determined PGE contents of subvolcanic rocks associated with the Chuquicamata porphyry Cu (Chile) and the Grasberg porphyry Cu-Au deposits (Indonesia) for comparison (Fig. 1). These results will be discussed together with literature data from the El Abra porphyry Cu system in Chile, the Northparkes and Cadia Au-Cu porphyry systems in Australia (Cocker et al. 2015; Hao et al. 2017; Lowczak et al. 2018), and the Bingham porphyry Cu-Au system in the USA (Maughan et al. 2002).

Geological settings and samples

Barren suites

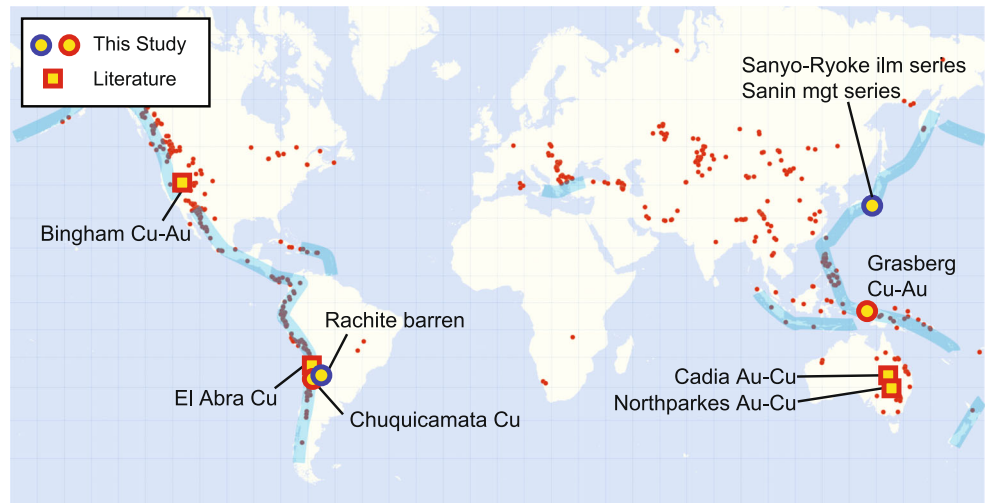
The Rachaite complex is a small calc-alkaline suite of basaltic andesite to dacite flows in northwest Argentina that erupted between 7.2 and 8.4 Ma (Kay et al. 2010). It includes some of the least evolved lavas in the northern Puna Volcanic Complex. Whole-rock major and trace element geochemistry and Sr, Nd, Pb, and O isotopic data suggest that these northern Puna volcanic rocks crystallized from hybrid magmas that formed by mixing of mantle-derived magmas with pelitic crustal melts in a 50 to 75 km, contractionally thickened crust (Kay et al. 2010). During ascent, the magma ponded at a depth of 20–25 km and underwent further assimilation-fractional crystallization (AFC). The Rachaite suite is associated with Pb, Zn, and Ag mineralization, but not with Cu or Au mineralization (Coira and de Brodtkorb 1995). Ten samples from Kay et al. (2010), which range from olivine-bearing basalt to glassy dacite, were analyzed for PGE and selected trace elements.

The Cretaceous-Paleogene granitoids in the Japan arc are classified into two groups, the reduced Ryoke and Sanyo ilmenite-series and the oxidized Sanin magnetite-series, based on their magnetic susceptibility (Kanaya and Ishihara 1973). The Ryoke and Sanyo suites are dominant in the southern parts of the Japan arc where the basement is mainly a Jurassic accretionary complex. In contrast, the Sanin magnetite-series granitic rocks are mainly distributed over the northern part of the arc (Takagi 2004). There are no porphyry deposits associated with the Cretaceous-Paleogene Japanese granitoids (Ishihara 2007), whereas the Sanin magnetite-series host Mo vein and Pb-Zn skarn deposits and the Sanyo-Ryoke granitoids are associated with W deposits and locally a few minor Cu skarn deposits (Ishihara 2007). Nine granitic samples from the Sanin suite and 11 samples from the Sanyo-Ryoke suite were analyzed in this study. Sample locations are reported in Electronic Supplementary Material (ESM) Fig. 1 and ESM Table 1.

Porphyry Cu \pm Au suites

The Chuquicamata porphyries, which host one of the largest porphyry Cu deposits in the Andes, are located at the southern end of the Chuquicamata Intrusive Complex. They intrude a pre-Cenozoic igneous, sedimentary, and metamorphic basement along the late Eocene to Oligocene West Fissure strike-slip fault zone (Ballard et al. 2001). The mineralized intrusive suite consists of the East, West, and Bench porphyries, which are composed of granodiorite, monzogranite, and monzodiorite. Six of the least altered samples from Ballard et al. (2001) were selected for this study.

Fig. 1 Locations of volcanic and subvolcanic rock suites included in this study. The red circles represent the locations of active porphyry copper mines (Singer et al. 2005). Thick light blue solid lines represent subduction zone



The Grasberg Cu-Au porphyry is the world's largest Au producer (Cooke et al. 2005). The deposit is situated within the Grasberg-Ertsberg porphyry-skarn mineralized district in the highlands of Papua, Indonesia. The Grasberg deposit is associated with a group of brecciated diorites to quartz monzonites intrusive units that form a pipe-shaped body, which intrudes the siliciclastic and carbonate units of the New Guinea Limestone Group (MacDonald and Arnold 1994; Leys et al. 2012). Five of the least altered samples from the Main Grasberg Intrusions, which are most closely associated with the Grasberg porphyry mineralization, and Kali intrusions were included in this study.

Analytical methods

Major and trace elements

Major and trace elements of some Rachaite samples were measured by EPMA and LA-ICP-MS at ANU using the method of Campbell (2003) and the results are reported in Electronic Supplementary Material (ESM Table 2). Synthetic glass beads were prepared using 0.375 g of sample powder and 0.75 g of lithium borate flux (12:22 $\text{Li}_2\text{B}_4\text{O}_7/\text{LiBO}_2$ mass ratio). The EPMA was performed by a CAMECA SX100 electron microprobe in WDS mode with the beam conditions of 15 kV and 20 nA. The LA-ICP-MS analysis was carried out at a laser repetition rate of 5 Hz with a spot size of 105 μm . Each spot analysis consisted of 30 s of background measurement followed by 40 s of sample ablation. The BCR-2g (USGS) standard was analyzed before and after analyses of 10 unknown samples. The NIST 612 was used to monitor quality control. Ca concentrations measured by XRF (Kay et al. 2010) or EPMA (this study) were used as an internal standard to determine the absolute concentrations of the elements. Analytical uncertainties obtained by multiple analyses of

NIST 612 were ± 1 to 4% (1σ) depending on the elements. Analytical accuracy is better than 10% for all elements, except for Cu (25%) and Cr (18%). The results are shown in ESM Table 3 where our measured values for NIST 612 are compared with the reference values from GeoReM database (Jochum et al. 2005).

PGE and Re

The whole-rock PGE and Re contents of the samples were determined by the Ni-sulfide fire assay-isotope dilution ICP-MS method described by Park et al. (2012b). The results are reported in Table 1. The sensitivities during analysis were $\sim 3 \times 10^5$ cps/ppb for mass 89, 140, and 205 using Agilent 7700x quadrupole ICP-MS at ANU. The Ir, Ru, Pt, Pd, and Re contents were measured by isotope dilution using the $^{99}\text{Ru}/^{101}\text{Ru}$, $^{191}\text{Ir}/^{193}\text{Ir}$, $^{195}\text{Pt}/^{194}\text{Pt}$, $^{105}\text{Pd}/^{108}\text{Pd}$, and $^{185}\text{Re}/^{187}\text{Re}$ ratios, respectively. Rhodium contents were determined by the method described in Meisel et al. (2003), which used the count rate of ^{103}Rh and ^{106}Pd assuming that the recovery rates of Rh and Pd were similar to each other during the analytical procedure. Molecular interferences on PGEs by Ni, Cu, Zn, Co, Hf, Mo, Zr, and Ta argides or oxides were monitored, and the effects of the interferences were corrected using measured oxide (0.3–0.4%) and argide production rate (0.003–0.006%). The interference on Ir, Pt, and Re by the metal oxide and argide is negligible. The interferences on ^{105}Pd and ^{108}Pd by $^{65}\text{Cu}^{40}\text{Ar}$, $^{68}\text{Zn}^{40}\text{Ar}$, $^{102}\text{Zr}^{16}\text{O}$, $^{102}\text{Mo}^{16}\text{O}$, and ^{108}Cd are corrected. The differences between data before and after the correction are $< 2\%$. There is significant interference on ^{101}Ru by $^{61}\text{Ni}^{40}\text{Ar}$. The differences for Ru ranges from 9 to $> 100\%$ due to low contents of Ru in samples. Procedural blanks were measured from the sample-free analysis. The average procedural blanks and the method detection limits that are taken as three standard deviations of the procedural blanks are reported in ESM Table 4. The accuracy and precision of the analyses were assessed by multiple measurements ($n = 7$)

Table 1 Platinum group element and Re concentrations in volcanic and subvolcanic rocks

Sample	MgO (wt.%)	Cu (ppm)	Ir (ppb)	Ru (ppb)	Rh (ppb)	Pt (ppb)	Pd (ppb)	Re (ppb)	Pd/MgO × 10 ⁹	Pd/Pt
Volcanic rocks from the Rachaite suite, Argentina										
P17-2A	1.80	10	0.0015	<0.0014	0.0016	0.039	0.080	0.019	0.044	2.0
P17-2B	1.89	15	0.0007	<0.0014	<0.0003	0.019	0.047	0.071	0.025	2.4
P17-3	0.77	11	<0.0003	<0.0014	<0.0003	<0.005	<0.009	<0.012	0.012	1.8
P17-5	1.54	4	<0.0003	<0.0014	<0.0003	<0.005	0.014	0.050	0.009	2.7
P17-7	1.50	7	<0.0003	<0.0014	<0.0003	<0.005	0.016	<0.012	0.010	3.1
RA95-1	2.20	11	0.0055	0.0086	0.0029	0.030	<0.009	0.079	0.004	0.3
RA95-2	3.54	17	0.0007	0.0066	<0.0003	0.015	0.032	<0.012	0.009	2.1
RA95-3	3.66	9	0.0014	0.0047	0.0012	0.033	0.017	0.012	0.005	0.52
P17-4	4.42	30	0.0098	0.0020	0.0011	0.071	0.046	0.066	0.010	0.65
P17-6	5.83	4	0.0281	0.0179	0.0183	0.344	0.214	0.038	0.037	0.62
Granitoids from the Sanyo-Ryoke-Sanin magmatic belt, Japan										
Sanyo-Ryoke magnetite-series										
SJ3	0.42	n.d.	0.0009	0.005	0.002	<0.018	0.035	0.064	0.082	
SJ5	0.15	n.d.	<0.0002	0.006	0.001	<0.018	0.004	0.116	0.024	
SJ5 duplicate	0.15	n.d.	0.0003	0.004	<0.0001	<0.018	0.004	0.147	0.023	
SJ6	0.96	n.d.	0.0004	0.003	0.0003	0.035	0.012	0.907	0.012	0.33
SJ6 duplicate	0.96	n.d.	<0.0002	<0.003	0.0003	0.070	0.010	0.838	0.010	0.14
SJ8	0.50	n.d.	0.0006	0.006	0.002	0.019	0.009	0.120	0.019	0.49
SJ9	0.60	n.d.	<0.0002	<0.003	0.0003	0.037	0.009	0.253	0.016	0.25
SJ10	3.10	n.d.	0.0006	0.008	0.005	0.025	0.020	0.234	0.007	0.80
SJ10 duplicate	3.10	n.d.	0.0004	0.030	0.008	0.023	0.020	0.402	0.007	0.89
SJ27	0.79	n.d.	0.0006	<0.003	0.001	0.023	0.008	0.107	0.010	0.33
SJ39	1.32	n.d.	0.0008	<0.003	0.003	<0.018	0.015	0.033	0.012	
SJ42-1	0.34	n.d.	0.0003	<0.003	0.002	0.019	0.008	0.347	0.024	0.41
Sanin ilmenite-series										
SJ11	5.98	n.d.	0.0002	0.004	<0.0001	<0.018	0.008	0.878	0.001	
SJ11 duplicate	5.98	n.d.	<0.0002	0.007	0.0003	<0.018	0.009	1.059	0.002	
SJ17	1.00	n.d.	0.0004	0.008	0.008	<0.018	0.014	0.256	0.014	
SJ17 duplicate	1.00	n.d.	0.0003	<0.003	0.003	<0.018	0.011	0.263	0.011	
SJ18	0.12	n.d.	0.0044	<0.003	0.0003	0.037	0.006	0.118	0.048	0.16
SJ18 duplicate	0.12	n.d.	0.0005	0.005	0.001	0.025	0.006	0.148	0.052	0.25
SJ22	0.13	n.d.	<0.0002	<0.003	0.000	0.148	0.008	0.098	0.060	0.05
SJ45	0.34	n.d.	0.0007	0.007	<0.0001	0.080	0.002	0.441	0.005	0.02
SJ50	1.45	n.d.	<0.0002	0.011	0.002	<0.018	0.004	0.021	0.003	
SJ50 duplicate	1.45	n.d.	<0.0002	<0.003	<0.0001	<0.018	<0.001	0.015	0.0007	
SJ51	5.91	n.d.	0.0003	<0.003	0.001	0.042	0.019	0.319	0.003	0.45
SJ54	1.93	n.d.	0.0028	0.004	0.003	0.091	0.231	0.338	0.120	2.5
SJ60	0.18	n.d.	<0.0002	0.006	0.033	<0.018	0.015	0.067	0.084	
SJ60 duplicate	0.18	n.d.	0.0003	<0.003	0.033	<0.018	0.013	0.059	0.069	
SJ61	1.05	n.d.	<0.0002	0.003	0.0005	0.037	0.005	0.513	0.005	0.15
SJ61 duplicate	1.05	n.d.	0.0005	<0.003	0.0003	0.020	0.011	0.438	0.011	0.56
SJ64-1	0.37	n.d.	0.0004	0.010	0.0002	<0.018	0.016	0.209	0.043	
SJ64-1 duplicate	0.37	n.d.	0.0004	<0.003	0.001	<0.018	0.018	0.237	0.049	
Subvolcanic rocks from the Chuquicamata porphyry Cu deposit, Chile										
98-508	0.56	397	<0.0003	<0.0014	<0.0003	0.019	0.057	1.00	0.102	3.0
98-511	0.63	2615	0.0030	0.0040	<0.0003	0.036	0.071	1.62	0.113	2.0
98-503	0.64	11,213	<0.0003	<0.0014	0.0015	0.031	0.031	6.28	0.048	1.0

Table 1 (continued)

Sample	MgO (wt.%)	Cu (ppm)	Ir (ppb)	Ru (ppb)	Rh (ppb)	Pt (ppb)	Pd (ppb)	Re (ppb)	Pd/MgO × 10 ⁹	Pd/Pt
98-601	0.42	1221	<0.0003	<0.0014	<0.0003	0.094	1.88	4.79	4.485	20.1
98-505	0.59	600	<0.0003	<0.0014	<0.0003	0.009	0.106	0.65	0.178	11.9
98-506	0.44	155	0.0025	<0.0014	<0.0003	0.015	0.080	0.79	0.182	5.2
Subvolcanic rocks from the Grasberg porphyry Cu-Au deposit, Indonesia										
Gras11	1.36								0.310	1.8
Gras2	1.45								0.426	1.8
Gras12	1.69								0.548	2.7
Gras13	2.27								1.852	2.0
Gras14	1.77								3.147	8.9

Numbers in italics are calculated using the limit of detection values

n.d. not determined

of reference material TDB-1. The results are shown in ESM Table 5. Reproducibility represented as the relative standard deviation (1σ) is < 10% for Pt, Rh, Ru, and Re for 14% for Pd and 23% for Ir. The measured values are consistent with previously reported values within 2σ .

Results and discussion

The major and trace element and PGE contents of the Chuquicamata Cu porphyry and Grasberg Cu-Au porphyry, obtained for this study, are presented in Table 1 and ESM Table 2. These results will be discussed and compared with those of previous studies on the El Abra Cu porphyry in Chile (Cocker et al. 2015), the Northparkes and Cadia Au-Cu porphyries in Australia (Hao et al. 2017; Lowczak et al. 2018), and the Bingham porphyry Cu-Au in the USA (Maughan et al. 2002).

Effect of alternation and mineralization

Because the emphasis of this study is on primary magmatic processes, the samples analyzed were the freshest possible. Nevertheless, some of the porphyry-related rocks used in this and previous studies contain some hydrothermal sulfides, including hydrothermal Cu. Furthermore, some mineralized porphyry systems are known to contain hydrothermal Pd and Pt (Economou-Eliopoulos 2005 and references therein), showing that hydrothermal fluids can mobilize Pd and Pt and, in rare cases, porphyry Cu deposits can contain up to 2400 ppb Pd (e.g., Skouries Cu porphyries, Greece; Economou-Eliopoulos and Eliopoulos 2000). However, empirical geochemical investigations (Yudovskaya et al. 2008; Tagirov et al. 2013; Zelenski et al. 2013, 2015; Park et al. 2016), supported by the results of experimental

and thermodynamic studies (Wood 1987; Sassani and Shock 1990; Fleet and Wu 1993, 1995; Taran et al. 1995; Hanley et al. 2005; Simon and Pettke 2009), show that the PGEs are normally appreciably less mobile than Cu and Re in magmatic-hydrothermal fluids.

The relative mobilities of Cu and Pd in the felsic suites considered in this study can be assessed from Fig. 2, which shows a plot of Cu against Pd for the porphyries associated with the Cu and Au-Cu deposits discussed in this paper. Copper varies by $\times 100$ in samples from the Chuquicamata Cu porphyry and by almost $\times 10,000$ in El Abra samples with no evidence of a correlated increase in Pd as might be expected if Pd was an important component in the hydrothermal

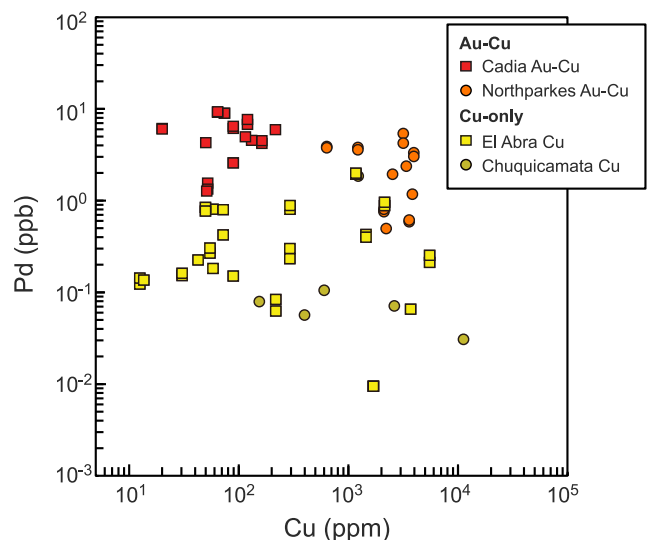


Fig. 2 Plot of Pd against Cu for the ore-bearing and barren suites included in this study. The Cadia, Northparkes, and El Abra data are from Lowczak et al. (2018), Hao et al. (2017), and Cocker et al. (2015) respectively

fluid. For example, the least mineralized sample from Chuquicamata (98–506), with 155 ppm Cu, and the most mineralized sample (98–503) with 11,213 ppm Cu, have similar PGE contents (Table 1). The Cu content of the samples from the Au-Cu deposits vary by only $\times 10$, so the influence of increasing Cu on Pd is less clear. What is clear is that there is no correlation between these elements and that samples from the Cu-rich Northparkes deposit contain less Pd than those from Cu-poor Cadia.

PGE geochemistry of ore-bearing suites

Figure 3 shows the Pd concentrations of the barren, Cu porphyry and Cu-Au porphyry suites plotted against MgO. The Pd contents of the volcanic and subvolcanic rocks associated with the Cadia and Northparkes Au-Cu suites are generally > 3 ppb and remain enriched until late in magma differentiation (< 1 wt.% MgO). The PGE contents of the highest MgO samples are comparable to those of primitive arc picrites and basalts (Fig. 3a), suggesting that they experienced little (Cadia) or no (Northparkes) sulfide segregation while fractionating in crustal magma chambers until a late stage of magma differentiation (Hao et al. 2017; Lowczak et al. 2018). Once the magma became sulfide-saturated PGE concentrations dropped rapidly due to their strong affinity for immiscible sulfide melts ($D^{\text{sul-sil}}_{\text{PGEs}} > \sim 1 \times 10^6$; Mungall and Brenan 2014). The Pd of the melt follows Cu and Au because all of these elements are incompatible with silicate and oxide minerals but strongly compatible with sulfide melts (e.g., Park et al. 2013, 2015). Therefore, the Cadia and Northparkes magmas, which reached sulfide saturation late in their history, had sufficient Cu and Au at the time of fluid exsolution to form Au-Cu ore deposits (Hao et al. 2017; Lowczak et al. 2018).

The Pd contents of intrusive rocks associated with the Chilean El Abra porphyry Cu deposit are seen to be consistently lower than those associated with the Australian porphyry Au-Cu deposits at the same MgO content (Fig. 3a). The decrease in the abundance of Pd seen in the El Abra samples with < 2.5 wt.% MgO suggests that sulfide segregation was taking place before the onset of volatile saturation which was placed at 1.1–1.5 wt.% MgO by Cocker et al. (2015). Cocker et al. (2015) further suggested that the El Abra magma formed a “Cu-only” porphyry deposit because small amounts of sulfide segregation during fractional crystallization before fluid saturation depleted the magma in the more chalcophile Au and not the less chalcophile Cu ($D^{\text{sul-sil}}_{\text{Au}} = \sim 1 \times 10^4$ and $D^{\text{sul-sil}}_{\text{Cu}} = \sim 1 \times 10^3$; Ripley et al. 2002; Mungall and Brenan 2014 and references therein).

The intrusive rocks associated with the Chuquicamata porphyry Cu deposit have similar Pd contents to the El Abra porphyries with the contents in both being at least an order

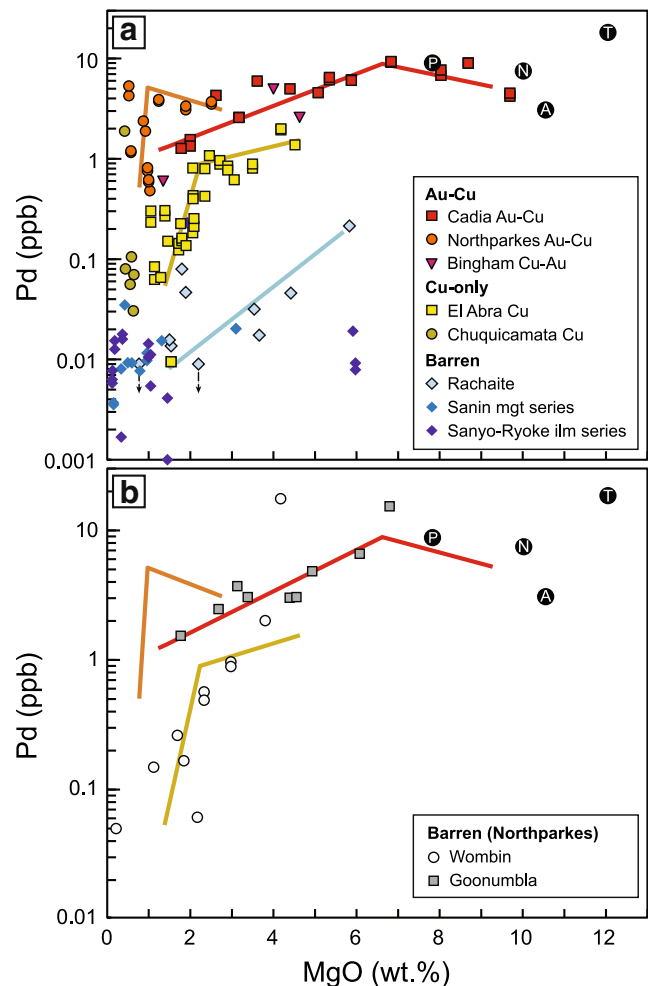


Fig. 3 **a** Plot of Pd against MgO for the ore-bearing and barren suites included in this study. The colored lines are references, which show variations in Pd during magma differentiation for each suite. The kinks in the reference lines show the point of sulfide saturation. Black dotted arrows represent data below the detection limit. Black circles with letters are average Pd contents for arc basalts and picrites with MgO contents between 8 and 14 from different localities. P = Pual Ridge basalt (sample MD3; Park et al. 2013), N = Niuatahi-Motutahi basalts (average of samples DG26-2 and DG26-3; Park et al. 2015), A = Ambae picrite (sample 68638; Park et al. 2012a), T = Tonga picrites (average of samples ND03-01 and 04-01; Dale et al. 2012). **b** Plot of Pd against MgO for the barren Wombin and Goonumbla suites from Northparkes. Reference lines for three of the ore-bearing suites in **a** are shown for comparison

of magnitude higher than those in barren suites at a similar wt.% MgO. This implies that the Chuquicamata magma had a chalcophile element budget similar to that of the El Abra magma at fluid saturation, which can explain why Chuquicamata is also a Cu-only deposit.

PGE geochemistry of barren suites

The PGE contents of barren rocks from the Rachaite suite, Argentina, and the Sanyo-Ryoke-Sanin suites, Japan, are

systematically depleted compared with the $\text{Cu} \pm \text{Au}$ ore-bearing igneous suites at the same MgO content (Fig. 3a and ESM Fig. 2). This suggests that either they have lost most of their chalcophile element budget by sulfide segregation at depth or that they originated from a chalcophile element-poor source. The Pd and Pt contents of the Rachaite volcanic rocks gradually decrease with decreasing MgO from 5.8 to 0.8 wt.% (Fig. 3a and ESM Fig. 2). These trends are different from those typically observed in sulfide-saturated magmatic systems in which Pd and Pt drop rapidly after sulfide saturation (Fig. 3 and ESM Fig. 2). As already noted, the Rachaite suite magmas were produced by mixing between mantle-derived basaltic and pelitic crustal melts (Kay et al. 2010). We performed mixing and AFC model following methods reported in Kay et al. (2010). The detailed conditions and parameters for the AFC model are in ESM Appendix I. The results show that the major and trace element geochemistry of the Rachaite suite is best explained by mixing between the mafic and the felsic end-members (Fig. 4 and ESM Fig. 3). The Pd variations for most samples can also be ascribed to mixing between the two end-members, although some show depletion in Pd/Nd and fall below the mixing curve, suggesting sulfide segregation may have occurred locally during mixing (Fig. 4). If magmas become locally equilibrated with sulfide melt, Pd will decrease markedly with no corresponding change in Nd or Rb due to the high $D^{\text{sul-sil}}\text{Pd} > \sim 1 \times 10^5$ (Mungall and Brenan 2014), resulting in low Pd/Nd and Pd/Rb ratios.

The Pd content of the mafic end-member, which is an order of magnitude lower than that of primitive arc magmas (Fig. 3a), suggests that the mafic magma has lost some chalcophile elements before mixing with the felsic crustal magma. We suggest that the Rachaite primary magma lost its fertility through a combination of early sulfide segregation in the lower crust and mixing with sulfide-saturated, a chalcophile element-poor felsic magma in a mid-crustal chamber. This process may have depleted the Rachaite magma in Au and Cu, but not in Pb and Zn as it hosts Cu-poor, Pb-Zn polymetallic deposits (Coira and de Brodtkorb 1995). The

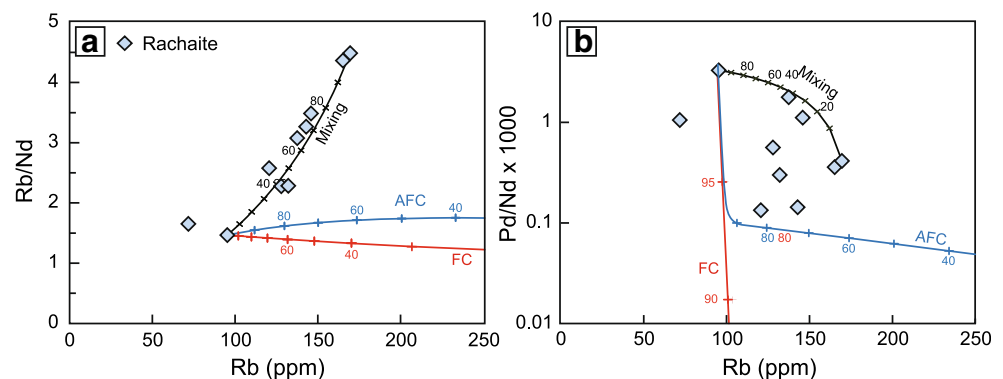
Rachaite case provides an example of how a chalcophile element-rich mantle-derived magma became barren during crustal evolution.

The Sanin-Sanyo-Ryoke granitoids, Japan, are characterized by marked depletion in all PGEs, including the mafic samples with > 3 MgO wt.% (Fig. 3a), which suggests that the Sanin-Sanyo-Ryoke magma may have either undergone extensive sulfide segregation in a mid-lower crustal magma chamber or that the primary magma was chalcophile element-poor. There have been several suggestions as to why there are no porphyry Cu deposits associated with the Cretaceous–Paleogene intrusive rocks of southeastern Japan, including shallow erosion depth and lack of thick continental crust (Qin and Ishihara 1998). However, our results show that the low chalcophile element fertility can be an important factor.

The Sanyo-Ryoke ilmenite-series granitoids are represented by high initial $^{87}\text{Sr}/^{86}\text{Sr}$ ratios between 0.7050 and 0.7106 and high $\delta^{18}\text{O}$ (> 8 ‰), suggesting the extensive involvement of crustal materials during their magma generation (Ishihara 2007 and references therein). The primary magma of the Sanyo-Ryoke ilmenite-series granitoids is interpreted to have formed by mixing between mantle-derived basaltic magma and partial melts of carbonaceous meta-sedimentary rocks (Ishihara 2007). Assimilation of sedimentary carbon into the magma will lower its oxygen fugacity and therefore its sulfur solubility. As a consequence, the Sanyo-Ryoke magmas are expected to leave sulfide in their source region following partial melting and to reach sulfide saturation early in their evolution. They are not prospects for Cu and Au mineralization.

The Sanin magnetite-series granitoids are interpreted to have originated from mantle-derived basaltic melt that assimilated carbon-poor meta-igneous basement rocks (Ishihara 2007). Their relatively low $\delta^{18}\text{O}$ (~ 5.5 – 8 ‰; Ishihara 2007), compared to those of the ilmenite-series, imply lesser amounts of crustal input during their genesis. The Sanin magnetite-series granitoids are oxidized relative to the ilmenite-series because they had little interaction with carbon-rich materials

Fig. 4 Mixing, AFC and FC modeling for plots of **a** Rb/Nd and **b** Pd/Nd against Rb for the Rachaite suite. Labeled markings on AFC and FC curves represent the percentage of melt (F) remaining in a system. Numbers on the mixing curves indicate the percentage of the mafic end-member in a system



during melting. This has led to the suggestion that they may have the potential for porphyry Cu deposits (Qin and Ishihara 1998). However, our results show that their chalcophile element depletion is similar to that of the ilmenite-series granitoids, which suggests that either the primary Sanin magma was deficient in chalcophile elements or that it was not sufficiently oxidized to exhaust all the sulfide phases in the source during melting.

Northparkes barren suites

The igneous rocks exposed around the Northparkes Au-Cu suites in Australia include two barren suites, the Goonumbra and Wombin Volcanics (Lickfold et al. 2003). These Middle to Upper Ordovician lavas occur associated with monzodioritic intrusions with a zircon U-Pb age of ~450 and 439 Ma, respectively (Butera et al. 2001). These ages coincide with the main Au-Cu mineralization period of the Northparkes deposit, which is between 445 and 437 Ma (Lickfold et al. 2003).

Figure 3b compares Pd variations in the Goonumbra and Wombin Volcanics with those of the Northparkes Au-Cu suites. The progressive depletion in Pd with decreasing MgO indicates that they have undergone early sulfide saturation and lost some Cu and Au to cumulus sulfide phases in a deep parental magma chamber (Hao et al. 2017). However, their Pd contents are still comparable to those of Cu- and Au-Cu suites at <3 wt.% MgO, implying some potential for forming a porphyry Cu ± Au deposit.

The evolution of the Goonumbra and Wombin suites are characterized by plagioclase-pyroxene fractionation whereas the Northparkes Au-Cu suites are dominated by plagioclase-amphibole fractionation (Hao et al. 2017). They are also not associated with porphyries or magmatic-hydrothermal alteration (Crawford et al. 2007). These observations suggest that Goonumbra and Wombin magmas were dry and may not

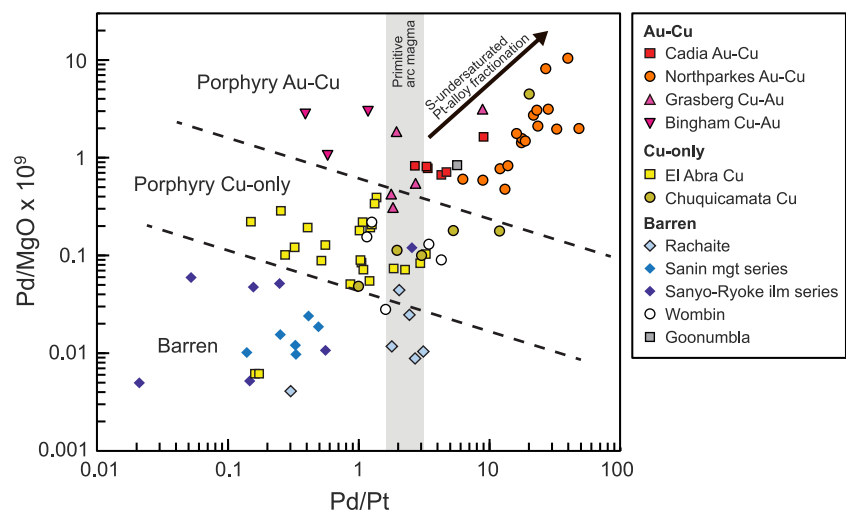
have experienced the extensive fluid exsolution required to form a porphyry Cu deposit despite their chalcophile element budgets being comparable to those of some other porphyry Cu ± Au suites. The Northparkes barren suites show that although the chalcophile element fertility is a critical factor, it is not the only factor required to form a porphyry Cu ± Au deposits.

Chalcophile element fertility indicator

This study shows that the PGE can be used as a tracer for Cu and Au and their geochemistry reflects changes in chalcophile element fertility during magma evolution, confirming the results of recent studies on the PGE geochemistry of felsic-intermediate igneous rock suites (Cocker et al. 2015; Park et al. 2015; Hao et al. 2017; Lowczak et al. 2018).

We suggest that plots of Pd/MgO against Pd/Pt are indicators of chalcophile element fertility and can be used to test its role in the formation of porphyry Cu ± Au deposits (Fig. 5). Palladium contents are normalized by MgO to correct for variations in Pd abundance caused by differences in fractional crystallization. The Pd/Pt ratio is used as a measure of the amount of fractional crystallization before sulfide saturation. This is because prior to sulfide saturation, Pd behaves incompatibly whereas Pt typically is sequestered by Pt-Fe alloys during fractionation of arc magma systems so that the Pd/Pt ratio increases with fractionation (Fig. 6a; e.g., Park et al. 2013, 2016). Once the magma becomes sulfide saturated, its Pd/Pt ratio begins to fall because Pd is more chalcophile than Pt (Fig. 6a; Park et al. 2016; Hao et al. 2017). The Northparkes and El Abra suites exhibit an abrupt decrease in Pd/Pt ratio after the onset of sulfide segregation (Fig. 6b). The seemingly opposite trend for the Cadia suite may be ascribed to their open system evolution (e.g., magma replenishment, Lowczak et al. 2018).

Fig. 5 Chalcophile element fertility diagram showing the difference between barren, Cu-only, and Cu-Au suites. Samples with <2.5 wt.% MgO were plotted except for the Cadia and Bingham suites, for which samples with <3.2 wt.% MgO and 1.4–4.6 wt.% MgO respectively were used. The barren, porphyry Cu, and porphyry Cu-Au bearing suites can be divided by dotted lines. The gray field represents a range of Pd/Pt values of primitive arc magmas (Dale et al. 2012; Park et al. 2012a, 2013, 2015)



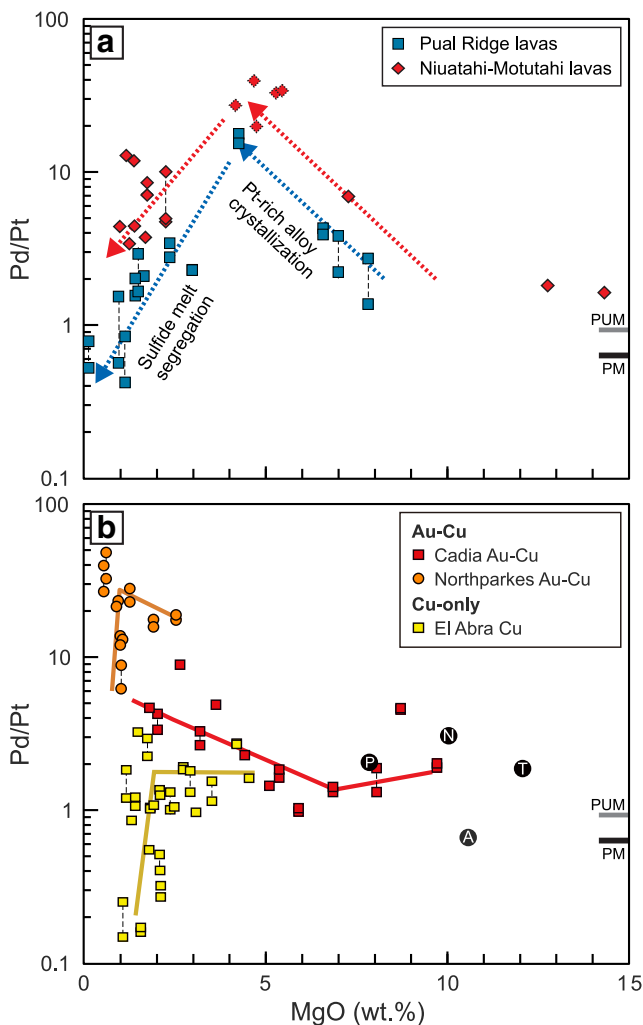


Fig. 6 Plot of Pd/Pt against MgO for **a** the Niuatahi-Motutahi lavas, Tonga rear arc (Park et al. 2015), and the Pual Ridge lavas, Eastern Manus Basin (Park et al. 2013) and **b** the Northparkes, El Abra, and Cadia suites. The Pd/Pt ratios of some Niuatahi-Motutahi lavas (diamonds with dotted line) are minimum estimation values obtained using Pd data of each sample and Pt data of DG26-3 in Park et al. (2015). Upward trending arrows result from Pt-rich alloy crystallization, downward trend lines sulfide melt segregation, and flat trend the absence of both alloy and sulfide precipitation. The primitive upper mantle (PUM) and primitive mantle (PM) values are from Becker et al. (2006) and McDonough and Sun (1995) respectively. P = Pual Ridge basalt (sample MD3; Park et al. 2013), N = Niuatahi-Motutahi basalts (average of samples DG26-2 and DG26-3; Park et al. 2015), A = Ambae picrite (sample 68638; Park et al. 2012a), T = Tonga picrites (average of samples ND03-01 and 04-01; Dale et al. 2012)

Bearing in mind that most porphyry Cu ± Au deposits are hosted by highly evolved andesitic to rhyolitic rocks, only samples with < 2.5 wt.% MgO are plotted on Fig. 5, which assumes that these low MgO samples are the most representative of the magma composition at the time of fluid saturation. Relatively mafic samples were included for the Cadia (< 3.2 wt.% MgO) and Bingham suites (1.4–4.6 wt.% MgO), as their Cu ± Au mineralization is

associated with andesitic intrusions (Lowczak et al. 2018; Maughan et al. 2002).

Low Pd/MgO and Pd/Pt ratios distinguish most barren suites from the ore-bearing suites (Fig. 5) and porphyry Cu from porphyry Cu-Au suites. Most of the Cu-Au suites have Pd/Pt ratios higher than those of primitive arc magmas, suggesting they have experienced prolonged sulfide-undersaturated fractionation or limited sulfide melt segregation (e.g., Cadia), which increased their chalcophile element fertility. The Goonumbla and Wombin barren suites have chalcophile element fertility similar to those of porphyry Cu suites but do not have Cu mineralization due to the low water content of their magmas.

Implications for the porphyry ore-forming process

The seminal study of Cline and Bodnar (1991) and recent numerical modeling studies (Chelle-Michou et al. 2017; Chiaradia and Caricchi 2017) argued that intrusion volume and duration of magma activity are the first-order factors controlling metal endowments, and particularly metal-enriched magmas are not essential for the genesis of economic porphyry Cu deposits. Chelle-Michou et al. (2017) suggested that any “normal” hydrous arc magmas have potential to produce fluids capable of forming porphyry Cu deposits and can form large porphyry deposits (> 20 Mt Cu) if they have long-lasting activity (> 1 Ma) and large volume (> 1000 km³) regardless of metal contents in a magma.

Two of the critical factors that control the economics of a porphyry system are its size and grade. The former is logically controlled by the size of the magma event associated with the hydrothermal mineralization and the latter by a combination of chalcophile element fertility and efficient transfer of metals from the melt to the fluid. Therefore, the higher the Cu and Au contents of the ore-associated magma at the time of volatile saturation, the higher the tenor of the ore for a given fluid/melt partition coefficient for Cu and Au. The ore grade and tonnage data for the porphyry deposits considered in this study are presented in Table 2. The Northparkes and Grasberg magmas, which have the highest chalcophile element fertility at fluid saturation (Fig. 5; Table 2), are associated with the highest Cu ore grades of > 1 wt.% among studied suites. Given the tonnage of the Northparkes deposit is ~0.15 Gt, which is at least an order of magnitude smaller than those of other porphyry deposits in this study (Table 2), the magma volume involved in the formation of the Northparkes deposit may have been at least an order of magnitude smaller than other deposits. However, the Northparkes magma formed an economically significant porphyry Au-Cu deposit (1.6 Mt Cu and 70 t Au; Cooke et al. 2007) due to high chalcophile element fertility. Magma composition appears to be particularly controlling the Au grade of a porphyry deposit. Figure 7 shows that the Au grades of porphyry ores are positively correlated with the Pd

Table 2 Tonnage, metal endowment, and grade of the porphyry Cu ± Au deposits included in this study and chalcophile element fertility indicators of the associated suites

Deposit	Tonnage (Gt)	Cu (Mt)	Au (t)	Cu (wt.%)	Au (g/t)	Au/Cu grade	Pd/Pt	Pd/MgO	References for the ore deposit data
Cu-only									
El Abra	1.8	8.8	18	0.49	0.01 ^a	0.02	1.2	0.2	1
Chuquicamata	7.5	66.4	301	0.55	0.04	0.07	7.2	0.9	2
Au-Cu									
Northparkes	0.15	1.6	70	1.03	0.46	0.45	22	2.5	3
Grasberg	2.5	30.5	2604	1.13	1.05	0.93	3.4	1.3	2
Cadia	1.3	4.4	1050	0.31	0.74	2.39	4.5	0.9	3
Bingham ^b	3.2	28.5	1227	0.88	0.38	0.43	3.2	0.7	2, 4

References: 1 = Singer et al. (2008), 2 = Cooke et al. (2005), 3 = Cooke et al. (2007), 4 = Maughan et al. (2002)

^a Assumed value, no information due to Au is not present in detectable concentrations (Singer et al. 2008)

^b Pd/Pt and Pd/MgO values were calculated by average of Tick-52A, 59A, and 69A from Maughan et al. (2002)

content of the magma at fluid saturation, as determined from the Pd content of the ore-associated porphyries. This observation suggests that the Au grade of the studied deposits is controlled by the Au contents of the magma at fluid saturation.

Mantle-derived arc magmas can be expected to undergo assimilation and fractional crystallization as they ascend through the crust and this will modify their compositions. The principal processes that control the Cu and Au contents in magmas at volatile exsolution are the relative timing of fluid and sulfide saturation. Furthermore, because Au is more

chalcophile than Cu, sulfide saturation leads to marked changes in the Au/Cu ratio of the melt. Figure 8 shows a theoretical model of the effect of sulfide saturation relative to fluid saturation using the Rayleigh fractionation equation after Cocker et al. (2015). Models 1 and 2 assume sulfide saturation at 30 and 70% fractionation, respectively, with an assumed sulfide melt fraction of 0.2 wt.% (e.g., Hao et al. 2017; Park et al. 2013, 2015) and gradual linear increase in the rate of sulfide segregation over a 10% fractionation interval (e.g., Keays and Tegner 2015). The sulfide melt and silicate melt partition coefficients ($D^{\text{sul-sil}}_{\text{Metal}}$) used for these models are 2×10^5 for Pd, 1×10^4 for Au, and 1.3×10^3 for Cu (Mungall and Brenan 2014 and references therein). Model 1 represents the Rachaite and Sanin-Sanyo-Ryoke cases (Fig. 8a). The magmas experienced early sulfide saturation due to the assimilation of reduced C-rich crustal materials and lost most of their chalcophile element and sulfur budget in cumulates within a deep crustal magma chamber. Their chalcophile element fertility was therefore low at the time of fluid saturation, which is assumed to occur long after sulfide saturation. Magmas from these suites are expected to be barren.

Model 2 represents suites associated with porphyry Cu ± Au deposits, such as those included in this study. If fluid saturation occurs at, or slightly after, 70% fractionation, the melts are enriched in both Cu and Au and therefore have the potential to form an Au-rich porphyry Cu deposit (Fig. 8b). It should be noted that 70% fractionation of a sulfide-undersaturated magma differentiation increases not only Cu and Au but also volatile elements such as S and Cl in the melt by more than a factor of three times the initial values, which will significantly improve the ore grade and reduce the duration and volume of magmatism required for economic porphyry Cu ± Au deposits. The PGE geochemistry of the Northparkes suite is consistent with this model (Fig. 3; Hao et al. 2017) and the high Pd/MgO and Pd/Pt ratios of the Grasberg samples (~ 1.5 wt.% MgO; Fig.

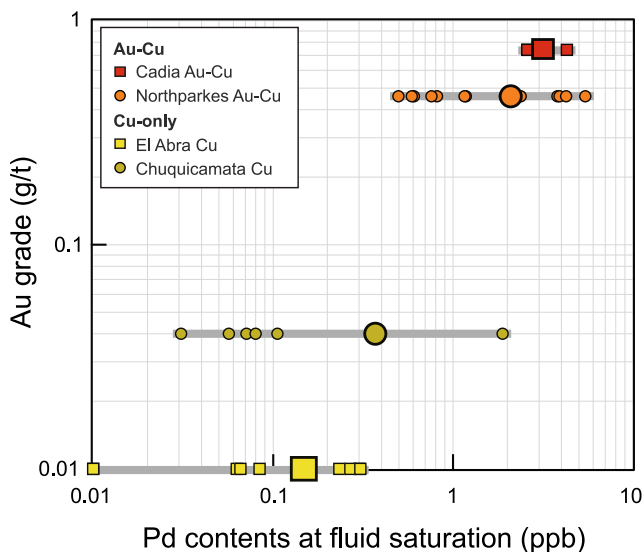


Fig. 7 Plot of Au grade in the ore against Pd concentration in the melt at fluid saturation. The large symbols represent the average of each suite. References for the Au grades are given in Table 2. MgO contents of the samples used to constrain the Pd concentrations in the melt at fluid saturation are 0.5–1.5 wt.% for the Northparkes (Hao et al. 2017), 1.0–1.5 wt.% for the El Abra (Cocker et al. 2015), 2.5–3.5 wt.% for the Cadia (Lowczak et al. 2018), and 0.4–0.7 wt.% for the Chuquicamata suite (this study)

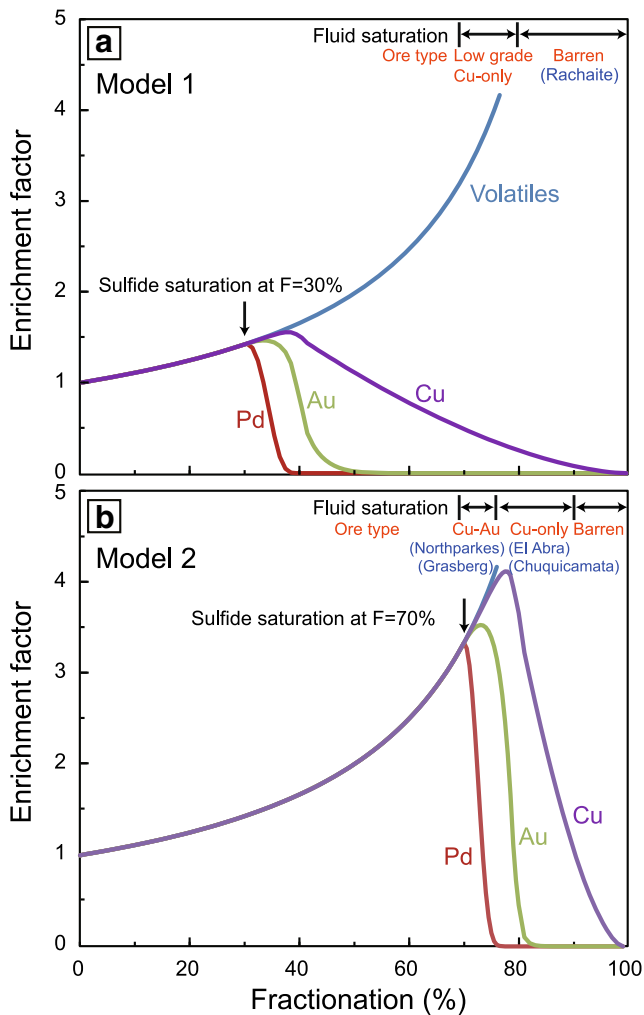


Fig. 8 Models simulating the Pd, Au, and Cu contents in the silicate melt as a function of fractionation with sulfide saturation at **a** 30% fractionation and **b** 70% fractionation. The single-headed arrow represents the assumed timing of sulfide saturation. The double-headed arrows represent the assumed timing of fluid exsolution and the expected ore types formed from the fluid

5) suggest that they also remained sulfide undersaturated until the final stages of magma differentiation.

If fluid saturation occurs after sulfide saturation at ~80% fractionation, the 10% fractionation interval between sulfide and fluid saturation can deplete the melt in Au without removing a significant amount of Cu because the partition coefficient of Au into an immiscible sulfide melt is about ten times higher than that of Cu (Mungall and Brenan 2014 and references therein; Fig. 8b). The result is a “Cu-only” deposit as seen in the El Abra (Cocker et al. 2015) and Chuquicamata suites (this study).

An apparent exception is Cadia, which reached sulfide saturation at 6.8 wt.% MgO (Fig. 3a), well before fluid saturation at ~3 wt.% MgO (Lowczak et al. 2018). Nevertheless, the Cadia magma retained enough Cu and Au to form a porphyry Au-Cu deposit due to a combination of the fraction of sulfide

melt to precipitate from the silicate melt (0.023 wt.%) being about a factor of ten less than other arc-related magmas (~0.2 wt.%; Hao et al. 2017; Park et al. 2013, 2015) and the *R* factor being less than D_{Au} ($R = \text{silicate melt/sulfide melt ratio} = 14,000$; Lowczak et al. 2018). The small fraction of sulfide melt segregation may be due to destabilization of the sulfide melt by interaction with volatile phases (e.g. Mungall et al. 2015).

The Cu and Au grades of the 37 largest known porphyry Cu and Au-Cu deposits (Cooke et al. 2005), including those investigated in this study, are presented in Fig. 9. For the giant porphyry Cu deposits (> 10 Mt Cu and Au/Cu grade < 0.1×10^{-3}), the Cu and Au grades are positively correlated regardless of the tonnage of each deposit, suggesting that the duration and volume of magma activity are not the primary controls on the ore grade. Note that as the Cu grade decreases from 1.2 to 0.3 wt.%, the Au grade shows almost two orders of magnitude depletion from ~0.4 to ~0.002 g/t. Fluid composition and emplacement depth have been considered to be significant factors controlling the ore grade and Au/Cu ratio (Murakami et al. 2010). However, we suggest that this trend can also be explained by variations in chalcophile element fertility due to differences in the interval between sulfide and fluid saturation in each deposit. To test this hypothesis, we calculated the Cu and Au grades of the ores precipitated from the fluid in equilibrium with the melt compositions predicted by model 2 assuming initial Cu and Au contents of 50 ppm and 4 ppb respectively (Lee et al. 2012; Park et al.

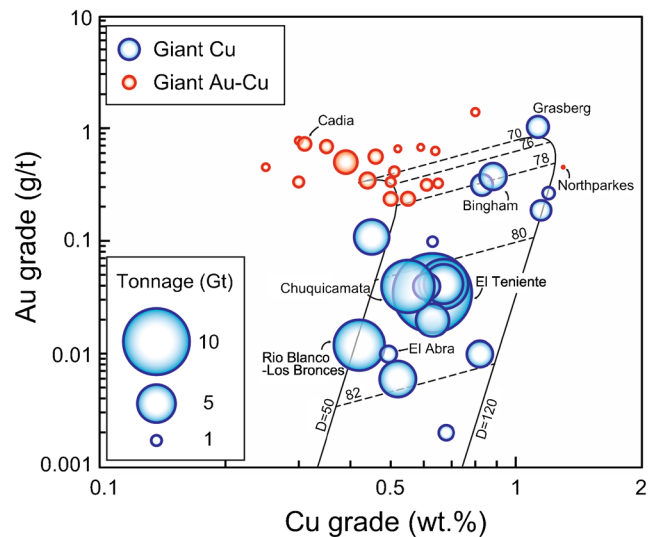


Fig. 9 Plot of Cu and Au grades in ores for giant porphyry deposits, including those investigated in this study. Names of ore deposits with tonnages of > 5 Gt are also shown. Data are from Cooke et al. (2005, 2007). The solid lines represent the Cu and Au grades of the ore formed from the fluid in equilibrium with the melt for model 2 in Fig. 7, assuming $D^{\text{fluid-melt}}_{Cu}$ and $D^{\text{fluid-melt}}_{Au}$ of 50–120 and precipitation efficiency of 50%. The dashed lines are fractionation (%) from model 2 in Fig. 7

2015). The trends of the ore grades of the giant porphyry Cu deposits can be best explained if fluid saturation occurs between 70 and 82% fractionation in model 2, with $D^{\text{fluid-melt}}_{\text{Cu}}$ and $D^{\text{fluid-melt}}_{\text{Au}}$ of 50–120 and precipitation efficiency of 50% (e.g., Chiaradia and Caricchi 2017). These D values compare well with experimentally determined values (Simon et al. 2006; Simon et al. 2007). The results show that as the interval between sulfide and fluid saturation increases, the Au grade abruptly decreases with the slight decrease of the Cu grade, supporting for the role of chalcophile element fertility in controlling the ore grade of the giant porphyry Cu deposits. Although this calculation has considerable uncertainty introduced by the assumptions, which include the initial metal contents, the timing and degree of sulfide melt segregation, and precipitation efficiency, the positive correlation between Cu and Au grades is not dependent on these assumptions. Note that the porphyry Au-Cu deposits do not show positive correlations between Cu and Au grades, which suggests that their genesis involved a particularly Au-rich magma source (e.g., Richards 2009) or fluid (e.g., Murakami et al. 2010).

Conclusion

This study investigated the systematic differences in PGE geochemistry of barren and porphyry Cu \pm Au suites. The results show that the barren suites are marked by substantial depletion in PGEs with low Pd/MgO ($< \sim 0.1 \times 10^9$) and Pd/Pt ($< \sim 3$) ratios whereas the Cu \pm Au suites are systematically enriched in PGEs with high Pd/MgO ($> \sim 0.1 \times 10^9$) and Pd/Pt (~ 0.1 –40) ratios at late stages of magma differentiation (< 2.5 wt.% MgO). The barren magmas commonly undergo early sulfide saturation, which substantially lowers their chalcophile element fertility. In contrast, the magmas associated with porphyry Cu \pm Au deposits are characterized by late sulfide saturation, which allows Cu and Au, as well as S, to be concentrated by fractional crystallization, increasing chalcophile element fertility.

We suggest that Pd/MgO and Pd/Pt ratio can be used as chalcophile element fertility indicators, which can distinguish barren suites from the Cu \pm Au suites. The positive correlations between these indicators and the ore grades, particularly for Au, suggest that the ore grades are controlled by magmatic Cu and Au contents, in combination with a fluid composition, as suggested by previous studies. Given that Au is a critical byproduct that improves the profitability of many porphyry Cu deposits, the PGE geochemistry-based chalcophile element fertility indicators, as outlined in this paper, will help identify Au-rich exploration targets.

Acknowledgements The authors would like to thank David Holwell and Jamie Wilkinson for their critical and constructive reviews and Wolfgang Maier for his valuable comments and editorial handling. This work was

supported by the Australian Research Council Discovery Grants to Ian Campbell. We also acknowledge the support from the Korea Government Ministry of Science, ICP and Future Planning (NRF-2015R1C1A1A01054101 and NRF-2017K1A1A2013180). Ryoji Tanaka is thanked for his assistance for field trips in Japan.

Open Access This article is distributed under the terms of the Creative Commons Attribution 4.0 International License (<http://creativecommons.org/licenses/by/4.0/>), which permits unrestricted use, distribution, and reproduction in any medium, provided you give appropriate credit to the original author(s) and the source, provide a link to the Creative Commons license, and indicate if changes were made.

References

- Audétat A, Simon AC (2012) Magmatic controls on porphyry copper genesis. In: Hedenquist JW, Harris M, Camus F (eds) *Geology and genesis of major copper deposits and districts of the world: a tribute to Richard H Sillitoe*, vol 16. Society of Economic Geologists, 553–572
- Ballard JR, Palin JM, Williams IS, Campbell IH, Faunes A (2001) Two ages of porphyry intrusion resolved for the super-giant Chuquicamata copper deposit of northern Chile by ELA-ICP-MS and SHRIMP. *Geology* 29(5):383–386
- Becker H, Horan MF, Walker RJ, Gao S, Lorand JP, Rudnick RL (2006) Highly siderophile element composition of the Earth's primitive upper mantle: constraints from new data on peridotite massifs and xenoliths. *Geochim Cosmochim Acta* 70(17):4528–4550
- Burnham CW (1967) Hydrothermal fluids at the magmatic stage. In: Barnes HL (ed) *Geochemistry of hydrothermal ore deposits*, vol. Holt Rinehart and Winston, 34–76
- Butera KM, Williams IS, Blevin PL, Simpson CJ (2001) Zircon U-Pb dating of early Palaeozoic monzonitic intrusives from the Goonumbla area, New South Wales. *Aust J Earth Sci* 48:457–464
- Campbell IH (2003) Constraints on continental growth models from Nb/U ratios in the 3.5 Ga Barberton and other Archaean basalt-komatiite suites. *Am J Sci* 303(4):319–351
- Chelle-Michou C, Rottier B, Caricchi L, Simpson G (2017) Tempo of magma degassing and the genesis of porphyry copper deposits. *Sci Rep* 7:40566. <https://doi.org/10.1038/srep40566>
- Chiaradia M, Caricchi L (2017) Stochastic modelling of deep magmatic controls on porphyry copper deposit endowment. *Sci Rep* 7:44523. <https://doi.org/10.1038/srep44523>
- Chiaradia M, Ulianov A, Kouzmanov K, Beate B (2012) Why large porphyry Cu deposits like high Sr/Y magmas? *Sci Rep* 2:685. <https://doi.org/10.1038/srep00685>
- Cline JS, Bodnar RJ (1991) Can economic porphyry copper mineralization be generated by a typical calc-alkaline melt. *J Geophys Res-Solid* 96(B5):8113–8126
- Cocker HA, Valente DL, Park J-W, Campbell IH (2015) Using platinum group elements to identify sulfide saturation in a porphyry Cu system: the El Abra porphyry Cu deposit, northern Chile. *J Petrol* 56(12):2491–2514
- Coira BL, de Brodtkorb MK (1995) Polymetallic mineralization associated with Cenozoic volcanism in Northern Puna, Argentina. In: PACRIM Congress 1995, The Australasian Institute of Mining and Metallurgy, Auckland, New Zealand
- Cooke DR, Hollings P, Walsh JL (2005) Giant porphyry deposits: characteristics, distribution, and tectonic controls. *Econ Geol* 100(5): 801–818
- Cooke DR, Wilson AJ, House MJ, Wolfe RC, Walshe JL, Lickfold V, Crawford AJ (2007) Alkalic porphyry Au-Cu and associated mineral deposits of the Ordovician to Early Silurian Macquarie Arc, New South Wales. *Aust J Earth Sci* 54(2–3):445–463

- Crawford AJ, Meffre S, Squire RJ, Barron LM, Falloon TJ (2007) Middle and late Ordovician magmatic evolution of the Macquarie Arc, Lachlan Orogen, New South Wales. *Aust J Earth Sci* 54(2–3):181–214
- Crocket JH (2000) PGE in fresh basalt, hydrothermal alteration products, and volcanic incrustations of Kilauea volcano, Hawaii. *Geochim Cosmochim Acta* 64(10):1791–1807
- Dale CW, Macpherson CG, Pearson DG, Hammond SJ, Arculus RJ (2012) Inter-element fractionation of highly siderophile elements in the Tonga Arc due to flux melting of a depleted source. *Geochim Cosmochim Acta* 89:202–225
- Economou-Eliopoulos M (2005) Platinum-group element potential of porphyry deposits. In: Mungall J (ed) *Exploration for platinum-group element deposits*, vol 35. Mineralogical Association of Canada, 203–245
- Economou-Eliopoulos M, Eliopoulos DG (2000) Palladium, platinum and gold concentration in porphyry copper systems of Greece and their genetic significance. *Ore Geol Rev* 16(1–2):59–70
- Fleet ME, Wu TW (1993) Volatile transport of platinum-group elements in sulfide-chloride assemblages at 1000 °C. *Geochim Cosmochim Acta* 57(15):3519–3531
- Fleet ME, Wu TW (1995) Volatile transport of precious metals at 1000°C—speciation, fractionation, and effect of base-metal sulfide. *Geochim Cosmochim Acta* 59(3):487–495
- Halter W, Heinrich C, Pettko T (2005) Magma evolution and the formation of porphyry Cu-Au ore fluids: evidence from silicate and sulfide melt inclusions. *Mineral Deposita* 39(8):845–863
- Hanley JJ, Pettko T, Mungall JE, Spooner ETC (2005) The solubility of platinum and gold in NaCl brines at 1.5 kbar, 600 to 800 °C: a laser ablation ICP-MS pilot study of synthetic fluid inclusions. *Geochim Cosmochim Acta* 69(23):5635–5637
- Hao H, Campbell IH, Park J-W, Cooke DR (2017) Platinum-group element geochemistry used to determine Cu and Au fertility in the Northparkes igneous suites, New South Wales, Australia. *Geochim Cosmochim Acta* 216:372–392
- Ishihara S (2007) Origin of the Cenozoic-Mesozoic magnetite-series and ilmenite-series granitoids in East Asia. *Gondwana Res* 11(1–2):247–260
- Jenner FE, O'Neill HSC, Arculus RJ, Mavrogenes JA (2010) The magnetite crisis in the evolution of arc-related magmas and the initial concentration of Au, Ag and Cu. *J Petrol* 51(12):2445–2464
- Jochum KP, Nohl L, Herwig K, Lammel E, Toll B, Hofmann AW (2005) GeoReM: a new geochemical database for reference materials and isotopic standards. *Geostand Geoanal Res* 29(3):333–338
- Kanaya H, Ishihara S (1973) Regional variation of magnetic susceptibility of the granitic rocks in Japan. *J Jap Ass Min Petr Econ Geol* 68:219–224
- Kay SM, Coira BL, Caffè PJ, Chen CH (2010) Regional chemical diversity, crustal and mantle sources and evolution of central Andean Puna plateau ignimbrites. *J Volcanol Geoth Res* 198(1–2):81–111
- Keays RR, Tegner C (2015) Magma chamber processes in the formation of the low-sulphide magmatic Au-PGE mineralization of the Platinova Reef in the Skaergaard Intrusion, East Greenland. *J Petrol* 56(12):2319–2339
- Lee CTA, Luffi P, Chin EJ, Bouchet R, Dasgupta R, Morton DM, Le Roux V, Yin QZ, Jin D (2012) Copper systematics in arc magmas and implications for crust-mantle differentiation. *Science* 336(6077):64–68
- Leys CA, Cloos M, New BTE, MacDonald GD (2012) Copper-Gold ± Molybdenum deposits of the Ertsberg-Grasberg district, Papua, Indonesia. In: Hedenquist J, Harris M, Camus F (eds) *Geology and genesis of major copper deposits and districts of the world: a tribute to Richard H Sillitoe*, Volume Special Publication Number 16, Society of Economic Geologists, Inc. 215–235
- Lickfold V, Cooke DR, Smith SG, Ullrich TD (2003) Endeavour copper-gold porphyry deposits, Northparkes, New South Wales: intrusive history and fluid evolution. *Econ Geol Bull Soc* 98(8):1607–1636
- Lowczak JN, Campbell IH, Cocker H, Park J-W, Cooke DR (2018) Platinum-group element geochemistry of the Forest Reef Volcanics, southeastern Australia: Implications for porphyry Au-Cu mineralisation. *Geochim Cosmochim Acta* 220:385–406
- Maughan DT, Keith JD, Christiansen EH, Pulsipher T, Hattori K, Evans NJ (2002) Contributions from mafic alkaline magmas to the Bingham porphyry Cu-Au-Mo deposit, Utah, USA. *Mineral Deposita* 37(1):14–37
- MacDonald GD, Arnold LC (1994) Geological and geochemical zoning of the Grasberg Igneous Complex, Irian Jaya, Indonesia. *J Geochem Explor* 50:143–178
- McDonough WF, Sun SS (1995) The composition of the earth. *Chem Geol* 120(3–4):223–253
- McInnes BIA, McBride JS, Evans NJ, Lambert DD, Andrew AS (1999) Osmium isotope constraints on ore metal recycling in subduction zones. *Science* 286(5439):512–516
- Meisel T, Fellner N, Moser J (2003) A simple procedure for the determination of platinum group elements and rhenium (Ru, Rh, Pd, Re, Os Ir and Pt) using ID-ICP-MS with an inexpensive on-line matrix separation in geological and environmental materials. *J Anal Atom Spectrom* 18(10):720–726
- Mungall JE (2002) Roasting the mantle: slab melting and the genesis of major Au and Au-rich Cu deposits. *Geology* 30(10):915–918
- Mungall JE, Brenan JM (2014) Partitioning of platinum-group elements and Au between sulfide liquid and basalt and the origins of mantle-crust fractionation of the chalcophile elements. *Geochim Cosmochim Acta* 125:265–289
- Mungall JE, Brenan JM, Godel B, Barnes SJ, Gaillard F (2015) Transport of metals and sulphur in magmas by flotation of sulphide melt on vapour bubbles. *Nat Geosci* 8(3):216–219
- Murakami H, Seo JH, Heinrich CA (2010) The relation between Cu/Au ratio and formation depth of porphyry-style Cu-Au±Mo deposits. *Mineral Deposita* 45(1):11–21
- Nadeau O, Williams-Jones AE, Stix J (2010) Sulphide magma as a source of metals in arc-related magmatic hydrothermal ore fluids. *Nat Geosci* 3(7):501–505
- Park J-W, Campbell IH, Eggins SM (2012a) Enrichment of Rh, Ru, Ir and Os in Cr spinels from oxidized magmas: evidence from the Ambae volcano, Vanuatu. *Geochim Cosmochim Acta* 78:28–50
- Park J-W, Hu ZC, Gao S, Campbell IH, Gong HJ (2012b) Platinum group element abundances in the upper continental crust revisited—new constraints from analyses of Chinese loess. *Geochim Cosmochim Acta* 93:63–76
- Park J-W, Campbell IH, Arculus RJ (2013) Platinum-alloy and sulfur saturation in an arc-related basalt to rhyolite suite: evidence from the Pual Ridge lavas, the Eastern Manus Basin. *Geochim Cosmochim Acta* 101:76–95
- Park J-W, Campbell IH, Kim J, Moon JW (2015) The role of late sulfide saturation in the formation of a Cu- and Au-rich magma: insights from the platinum group element geochemistry of Niutahi-Motutahi lavas, Tonga rear arc. *J Petrol* 56(1):59–81
- Park J-W, Campbell IH, Kim J (2016) Abundances of platinum group elements in native sulfur condensates from the Niutahi-Motutahi submarine volcano, Tonga rear arc: implications for PGE mineralization in porphyry deposits. *Geochim Cosmochim Acta* 174:236–246
- Qin KZ, Ishihara S (1998) On the possibility of porphyry copper mineralization in Japan. *Int Geol Rev* 40(6):539–551
- Richards JP (2003) Tectono-magmatic precursors for porphyry Cu-(Mo-Au) deposit formation. *Econ Geol Bull Soc* 98(8):1515–1533
- Richards JP (2009) Postsubduction porphyry Cu-Au and epithermal Au deposits: products of remelting of subduction-modified lithosphere. *Geology* 37(3):247–250
- Ripley EM, Brophy JG, Li CS (2002) Copper solubility in a basaltic melt and sulfide liquid/silicate melt partition coefficients of Cu and Fe. *Geochim Cosmochim Acta* 66(15):2791–2800

- Sassani DC, Shock EL (1990) Speciation and solubility of palladium in aqueous magmatic-hydrothermal solutions. *Geology* 18(10):925–928
- Simon AC, Pettke T (2009) Platinum solubility and partitioning in a felsic melt-vapor-brine assemblage. *Geochim Cosmochim Acta* 73(2):438–454
- Simon AC, Pettke T, Candela PA, Piccoli PM, Heinrich CA (2006) Copper partitioning in a melt-vapor-brine-magnetite-pyrrothite assemblage. *Geochim Cosmochim Acta* 70(22):5583–5600
- Simon AC, Pettke T, Candela PA, Piccoli PM, Heinrich CA (2007) The partitioning behavior of As and Au in S-free and S-bearing magmatic assemblages. *Geochim Cosmochim Acta* 71(7):1764–1782
- Singer DA, Berger VI, Moring BC (2005) Porphyry copper deposits of the world: database, map, and grade and tonnage models. In, vol. U.S. Geological Survey pp Open-File Report 2005–1060
- Singer DA, Berger VI, Moring BC (2008) Porphyry Copper Deposits of the World Database and grade and tonnage models, 2008: U.S. Geological Survey Open-File Report 2008, 1155, 45 pp
- Tagirov BR, Baranova NN, Zotov AV, Akinfiyev NN, Polotnyanko NA, Shikina ND, Koroleva LA, Shvarov YV, Bastrakov EN (2013) The speciation and transport of palladium in hydrothermal fluids: experimental modeling and thermodynamic constraints. *Geochim Cosmochim Acta* 117:348–373
- Takagi T (2004) Origin of magnetite- and ilmenite-Series granitic rocks in the Japan arc. *Am J Sci* 304:169–202
- Taran YA, Hedenquist JW, Korzhinsky MA, Tkachenko SI, Shmulovich KI (1995) Geochemistry of magmatic gases from Kudryavy Volcano, Iturup, Kuril Islands. *Geochim Cosmochim Acta* 59(9):1749–1761
- Wilkinson JJ (2013) Triggers for the formation of porphyry ore deposits in magmatic arcs. *Nat Geosci* 6(11):917–925
- Wood SA (1987) Thermodynamic calculations of the volatility of the platinum group elements (PGE)—the PGE content of fluids at magmatic temperatures. *Geochim Cosmochim Acta* 51(11):3041–3050
- Yudovskaya MA, Tessalina S, Distler VV, Chaplygin IV, Chugaev AV, Dikov YP (2008) Behavior of highly-siderophile elements during magma degassing: a case study at the Kudryavy volcano. *Chem Geol* 248(3–4):318–341
- Zelenski ME, Fischer TP, de Moor JM, Marty B, Zimmermann L, Ayalew D, Nekrasov AN, Karandashev VK (2013) Trace elements in the gas emissions from the Erta Ale volcano, Afar, Ethiopia. *Chem Geol* 357:95–116
- Zelenski M, Taran Y, Galle B (2015) High emission rate of sulfuric acid from Bezymianny volcano, Kamchatka. *Geophys Res Lett* 42(17):7005–7013